

Enhanced magnetoelectric coupling in two-dimensional hybrid multiferroic heterostructures

Xilong Xu,¹ Li Yang*,^{1,2}

¹Department of Physics, Washington University in St. Louis, St. Louis, Missouri 63130, USA

²Institute of Materials Science and Engineering, Washington University in St. Louis, St. Louis, Missouri 63130, USA

Abstract

Magnetoelectric coupling in insulating multiferroic materials is invaluable for both fundamental research and multifunctional device applications. However, material realization remains a significant challenge. We employ first-principles calculations to predict an enhanced and stacking-robust magnetoelectric coupling in a multiferroic van der Waals heterostructure consisting of CrCl_3 and CuCrP_2S_6 . Within this heterostructure, the intralayer ferroic orders exhibit characteristics of a type-I multiferroic, while the interlayer ferroic orders resemble those of a type-II multiferroic, thus creating a hybrid-type multiferroic. Notably, the interlayer magnetic configuration can be switched upon electric polarization reversal, while maintaining the insulating property without any nontrivial phase transitions. Our analysis reveals a strongly interfacial spin local-field effect and proximity polarization effect on band alignments. These factors work synergistically to decide the interlayer exchange interaction and drive enhanced magnetoelectric coupling. Finally, we show that this magnetoelectric effect is robust in multi-layer structures, exhibiting a dependence on the layer number's parity. This research offers promising prospects for discovering enhanced magnetoelectric couplings in hybrid multiferroic van der Waals heterostructures.

*E-mail: lyang@physics.wustl.edu

The magnetoelectric (ME) effect, allowing for the effective manipulation of magnetism through an electric field and vice versa in multiferroic materials, holds immense promise in energy-efficient devices, spanning information storage, spintronic devices, memory, and magnetic sensors [1-6]. Traditionally, multiferroics are categorized into two types according to their ME couplings [7,8]. In Type-I multiferroics, where ferromagnetism (FM) and ferroelectricity (FE) have independent origins, ME coupling tends to be weak [9,10]. On the other hand, Type-II multiferroics exhibit strong ME coupling, as FE ordering consistently coincides with a magnetic transition [11-15]. However, achieving this significant coupling often involves challenges such as the stringent material specifications, weak FE polarization, and relatively low working temperature [16,17]. Despite extensive research efforts, identifying robust multiferroic materials with enhanced ME coupling remains a considerable challenge.

Recently, van der Waals (vdW) multiferroic heterostructures have garnered increasing research interest [18-28]. For example, the magnetic anisotropic energy (MAE) of CrGeTe₃ can be tuned by attaching FE In₂Se₃ [29]. In bilayer CrI₃, the interlayer magnetic order can be adjusted by attaching FE Sc₂CO₂ or In₂Se₃, where the FE component serves as a gating field to tune the interlayer band alignment of magnets [30-33]. However, these predictions either rely on charge-transfer effects, leading to emerging metallic states and unfavored leakage current, or are based on calculations of specific interlayer supercell structures due to lattice mismatch and considerable strain. More recently, intrinsic ME coupling via FE and antiferroelectricity (AFE) orders has been proposed, but switching between FE and AFE orders remains challenging [34].

In this study, we predict that the lattice-matched CrCl₃/CuCrP₂S₆ (CCPS) heterostructure exhibits enhanced insulating ME coupling. The interlayer magnetic configuration efficiently switches between FM and antiferromagnetic (AFM) couplings by altering FE polarization of CCPS. This effect remains robust across different interlayer stacking styles of the widely observed monoclinic phase. We elucidate two mechanisms: a unique spin local-field effect, where the switch in electric polarization significantly alters the spin component of interfacial chalcogen atoms and interlayer superexchange paths, and a substantial variation in band alignment induced by proximity electric polarization, modifying the hopping energy of interlayer superexchange interactions. These two factors synergistically enhance the overall ME effect. Finally, beyond bilayer, we predict a layer-dependent ME effect in multilayer heterostructures.

The first-principles simulations are performed using the Vienna ab initio Simulation Package (VASP) [35]. The atomic structure optimization is performed within the generalized gradient approximation (GGA) and Perdew–Burke–Ernzerhof (PBE) exchange-correlation functional [36,37] until the force on each atom is less than 0.02 eV/Å. To better capturing the correlation effects and underestimated band gaps by density functional theory (DFT), the electronic structure calculations are calculated by the hybrid functional theory (HSE06) [38,39]. Meanwhile, DFT+U calculations have been done, and the main results are not changed within the reasonable range of U values [40,41]. The k-mesh is set to 7 x 7 x 1 with a 450-eV cutoff energy. Dipole moment correction is employed [42], and the DFT-D3 method is employed to include vdW interactions [43]. Spin-orbit coupling (SOC) is included in the total-energy calculations. The FE transition pathway and energy barrier are calculated based on the nudged elastic band (NEB) approach [44]. The polarization is calculated by the modern polarization theory [45,46], and it hardly changes with the numbers of layers and calculation methods. [41] (see Section I of supplementary information for more simulation details).

The exchange coupling J between magnetic moments can be evaluated by the perturbation theory [47-50]. The basic form is

$$J = \frac{\langle S_i | H_{ij} | S_j \rangle}{E_j - E_i}, \quad (1)$$

where S_i and S_j represent the spin states I and j , respectively, E_i and E_j denote the corresponding energy levels. H_{ij} represents the hopping Hamiltonian. From this equation, we can elucidate that the exchange coupling is determined by the hopping integral in the numerator, *i.e.*, the spin wavefunction overlap, and the hopping energy in the denominator, *i.e.*, the energy difference between states. In traditional bulk type-I multiferroic structures, which are periodic, electronic structures are degenerate under opposite FE polarizations, indicating neither the hopping integral nor hopping energy is changed. As a result, the ME coupling is usually weak. However, 2D vdW heterostructures made by different layered materials break such a degeneracy along the out-of-plane direction. Particularly, the exceedingly thin nature and subsequent proximity effect around interface may amplify electric-polarization impacts, *e.g.*, the switch of FE polarization can significantly tune the interlayer band alignment and denominator in Eq (1). Meanwhile, the overlap between interlayer wavefunctions may also be modified subsequently, influencing the numerator in Eq (1). If these two factors can work synergistically, the overall interlayer magnetic order can be switched, giving hope to enhanced ME coupling.

Building upon this concept, we have taken the initiative to practically realize it through first-principles calculations. In the following, we propose a 2D vdW heterobilayer consisting of monolayer CrCl_3 and CCPS, as depicted in Figs. 1(a) and 1(b), respectively, to achieve enhanced ME coupling. Monolayer CrCl_3 , a member of chromium trihalides [51], manifests as a vdW insulating magnet. Each Cr ion holds a $3\text{-}\mu_{\text{B}}$ in-plane magnetic moment. The intralayer magnetic order is FM, while the interlayer order is observed to be AFM [52]. The other layer of this heterostructure is CCPS, which is a member of extensively studied metal phosphorus trichalcogenides [53]. Fig. 1(b) illustrates its crystal structure, featuring a $3\text{-}\mu_{\text{B}}$ in-plane moment on each Cr ion. Notably, CCPS exhibits an out-of-plane FE polarization due to off-center Cu ions, categorizing itself as a type-I multiferroic material. Both CCPS and CrCl_3 demonstrate insulating behaviors, characterized by band gaps of 2.4 eV and 3.7 eV, respectively [53,54]. Recent experiments have successfully obtained their monolayer structures, unveiling intriguing magneto-optical and FE properties [55,56].

Thanks to the minor lattice mismatch ($0.2\% \sim 0.7\%$) [51,53], we construct the $\text{CrCl}_3/\text{CCPS}$ heterostructure in Fig. 1(c). The HSE simulation reveals that this multiferroic heterostructure exhibits both FE and magnetic orders simultaneously. Under a downward electric polarization of CCPS, the ground-state interlayer magnetic coupling is in-plane AFM. Because of the net magnetic moment of a unit cell of CrCl_3 is $6 \mu_{\text{B}}$ (from two Cr ions) and that of CCPS is $3 \mu_{\text{B}}$, the net magnetization is not zero but $3 \mu_{\text{B}}$. The energy difference between the interlayer FM and AFM orders is approximately 0.25 meV per unit cell. This value is comparable to that of high-temperature (HT)-phase bilayer CrI_3 (~ 0.5 meV), which results in the observed interlayer AFM order [57,58]. Thus, this AFM order can be observed in similar experiments.

Upon switching the out-of-plane polarization of CCPS to the upward direction, we find that the ground-state interlayer magnetic coupling transitions to FM, accompanied by an energy gain of 0.24 meV/unit cell. The electric polarization can tune the relative magnetic energies by about 0.5 meV, which indicates the significant change for magnetic exchange interactions. Further exploration of the transition path in this heterostructure using the nudged elastic band (NEB) method, [44] as depicted in Fig. 1(d), yields an energy barrier of approximately 48 meV, aligning well with those typical values observed in FE materials [59] without the meta-stable paraelectric state [60]. Finally, the HSE band-structure calculations of those intermediate and final structures along the NEB path [41] affirm the preservation of a finite band gap (larger than 1.6

eV), a critical aspect supporting the insulating ME coupling. (see Section II of supplementary information) This feature is pivotal for experimental implementation, enabling the application of a gate electric field while minimizing the harmful leakage current.

It is known that the interlayer magnetic order is sensitive to the interlayer stacking style. There are six high-symmetry stackings styles in the CrCl₃/CCPS heterostructure. AA, AB₁, and AB₂ are originated from the rhombohedral phase, which is usually called the low-temperature (LT) phase in bulk chromium trihalides. AA', AB₁', and AB₂' are originated from the monoclinic phase, which is known as the HT phase [41]. Our above calculation is based on the AB₁ stacking. We have checked the ME effect of all other interlayer configurations and summarize the result in Section III of supplementary information [41]. All stacking styles exhibit ME coupling except the LT AB₂-stacking style. In practice, experimental annealing and stacking procedures significantly influence the fabricated interlayer configurations. Most fabricated van der Waals (vdW) magnets are observed in the high-temperature (HT) phase [57,58,61], which encompasses the AA', AB₁', and AB₂' stackings. The energy differences among these stackings are typically small, approximately 3 or 1 meV. Thus, our predicted ME effect is expected robust in fabricated CrCl₃/CCPS heterostructures.

Finally, we estimate the ME coupling to be about 1.25×10^{-10} s/m. This value is comparable with those of traditional ME materials, such as MgO/Fe/Au (9.4×10^{-11} s/m), P(VDF-TrFE)/Co/Pt (4×10^{-10} s/m), and BiFeO₃ (2.1×10^{-9} s/m) [62-64]. Moreover, the curie temperatures of CrCl₃ and CCPS are 17 K and 24 K, respectively, which are comparable with other two-dimensional materials, such as CrBr₃ (27 K) [65], Cr₂Ge₂Te₆ (30 K) [66], and MnBi₂Te₄ (25 K) [67].

In the following, we present the mechanisms inducing this enhanced ME coupling. Eq (1) shows that the magnetic coupling depends on both hopping integral and hopping energy. To analyze them, a clear understanding of the exchange interaction (hopping) paths is crucial, and we still choose the AB₁ stacking as an example to keep consistence with Fig. 1. The mechanisms are similar for other stacking styles.

Previous studies have demonstrated that the interlayer exchange interactions of vdW materials are mediated by interfacial non-magnetic atoms, so-called super-super-exchange interaction [68]. For both CrCl₃ and CCPS materials, due to the C_{3v} symmetry under the octahedral crystal field, their five degenerate *d* orbitals of Cr ions split into two subsets (i.e., two-fold *e_g* levels with a higher energy and three-fold *t_{2g}* levels with

a lower energy). In the case of Cr ions with a $3\mu_B$ magnetic moment, all t_{2g} orbitals are half-occupied, and two super-super-exchange paths can be identified [69]. Taking the AB_1 stacking as an example, the schematics of two interlayer super-super-exchange path are shown in Figs. 2(a) and 2(c). In Fig. 2(a), the Path-I coupling involves a hopping between two half-occupied t_{2g} orbitals through the participation of two π bindings of between Cr ions and interfacial nonmagnetic atoms. Importantly, the Cr-S-Cl path forms an angle of 112 degrees, close to 90 degrees. As discovered in previously works [39,69], this nearly orthogonal t_1 and t_π hoppings involve opposite spins of interfacial sulfur atoms, resulting in an AFM coupling. The corresponding schematic hopping path in the $CrCl_3/CCPS$ heterostructure is presented in Fig. 2(b). In contrast, Fig. 2(c) illustrates the other interlayer interaction, Path-II. It is between a half-occupied t_{2g} orbital and an empty e_g orbital through the involvement of one π binding and one σ binding of Cr ions with nonmagnetic interfacial atoms, which leads to a FM coupling due to the local Hund rules [48,70]. Different from Path-I, the Cr-S-Cl hopping in Path-II is 167 degrees, close to 180 degrees. Importantly, because t_σ and t_2 hoppings are nearly along the same direction, they are mediated by the same spin of the p orbital of interfacial sulfur atoms, as plotted in Fig. 2(d). The observed interlayer magnetic order emerges from the competition between these two distinct interlayer orbital exchange paths. There is also a third path shown in Section VI of supplementary information. [41] It has the same spin and orbital hoppings as Path-II, contributing to interlayer AFM coupling.

The reversal of FE polarization substantially impacts above hopping paths. As plotted in the left panel of Fig. 3(a), when electric polarization is downwards, both spin components are significant around interfacial sulfur atoms. In this scenario, Path-I exchange interaction becomes dominant due to the small energy difference between half-occupied t_{2g} orbitals of two components, and the system favors AFM coupling. Conversely, when electric polarization is switched upwards, the left panel of Fig. 3(b) shows that there is mainly the spin-down wavefunction (blue color) around interfacial sulfur atoms while the spin-up component is nearly depleted (right panel of Fig. 3 (b)). This is elucidated in Fig. 3(c): for upward polarization, the interlayer t_1 hopping of Path-I is substantially quenched due to depletion of the spin-up component, reducing AFM coupling. In contrast, for the FM hopping of Path-II shown in Fig. 3 (d), the interlayer t_2 hopping is almost not affected because it is mediated by the spin-down component of interfacial sulfur atoms. Therefore, the overall competition favors FM coupling under upward polarization. This spin local-field effect is essentially a surface

effect enhanced by the huge interface/volume ratio of vdW heterostructures, a feature unattainable in traditional bulk structures.

The other factor influencing the ME effect is the hopping energy, which is the denominator of Eq (1). In 2D out-of-plane FE materials, a significant proximity electric field is generated, and the switch of FE polarization changes the interlayer band alignment. We present the projected density of states in Fig. 4. First, we focus on the AFM Path-I coupling. Under the downward FE polarization shown in Fig. 4(a), the heterostructure exhibit a type-I band alignment with band gap of 2.1 eV. The AFM exchange Path-I is marked between occupied Cr-d- t_{2g} orbitals of CCPS and CrCl₃. After switching FE polarization to upward (Fig. 4(b)), the heterostructure is altered to be a type-II band alignment with a band gap of 1.6 eV. It is important to see that the energy difference between those occupied Cr-d- t_{2g} orbitals of CCPS and CrCl₃ is increased in Fig. 2(b), effectively reducing the strength of AFM Path-I coupling. In contrast, for the FM Path-II coupling marked in Figs. 4(c) and 4(d), the energy difference (\sim band gap) is reduced from 2.1 eV to 1.6 eV when switching FE polarization, effectively enhancing FM coupling. As a competition result, the overall ground-state magnetic coupling tends to switch from AFM to FM, which agrees with the first-principles result. It is worth noting that these two factors, the local-field induced changes of hopping integral and band-alignment associated hopping energies work in a synergistic way. For example, the upward polarization favors the FM hopping because of both the reduced hopping energy and its almost unaffected exchange FM Path-II.

As presented in the introduction, multiferroic materials are typically categorized to type-I or type-II. In this vdW heterostructure, the coexistence of intralayer FM order and out-of-plane FE polarization within CCPS is a typical type-I multiferroic because the FE order is from off-center Cu ions while the magnetism is from Cr ions. On the other hand, the interlayer magnetic order is decided by multiple factors, such as the atomic structure, chemical environment around the surficial atoms, and electric polarization. Thus, it exhibits characteristics more akin to a type-II multiferroic, consistent with the enhanced ME coupling. However, it doesn't belong to a typical type-II multiferroic structures, such as NiI₂ [17,71,72]. More accurately, it exhibits that the ferroelectricity simply selects the ground-state interlayer magnetic order. Moreover, unlike the traditional type-II multiferroic materials, which usually exhibit very weak electric polarization, both magnetic order and polarization of the CrCl₃/CCPS heterostructure are significant. For example, the out-of-plane electric polarization is about 0.8 $\mu\text{C cm}^{-2}$, which is about two orders of magnitude larger than those of typical

type-II multiferroic materials [17,71,72]. In this sense, the whole vdW heterostructure can be regarded as a hybrid multiferroic material.

It is worth mentioning that this hybrid multiferroics is a general phenomenon in vdW heterostructures because of the coexistence of interlayer and intralayer orders and huge interface/volume ratio, such as in $\text{CrBr}_3/\text{CuCrP}_2\text{S}_6$ and $\text{CrCl}_3/\text{CuVP}_2\text{S}_6$ heterostructure in Table S6. However, the enhanced ME coupling, which is strong enough to switch the ground-state magnetic order by FE polarization, is specific and rare. Its occurrence depends on the detailed competition of energy differences and the strength of interlayer exchange couplings of the materials involved. (see section VII of supplementary information) For material search, there are a few general principles that aid in achieving enhanced ME coupling. First, a small energy difference (e.g., less than 0.5 meV/unit cell) between FM and AFM orders is advantageous since it falls within the range of polarization-induced energy variations. Second, a highly tunable band alignment is preferred because it can be effectively modulated by out-of-plane polarization, changing the denominator term of exchange interactions.

Finally, we go beyond the bilayer heterostructure and study multilayer $\text{CrCl}_3/\text{CCPS}$ heterostructures, which are relevant for experimental interests. We focus on the layer dependence of the CrCl_3 part. The first-principles HSE results are summarized in Fig. 5(a). Regardless of the layer number of CrCl_3 , the ME effect is robust; the upward polarization favors a FM coupling, and the downward polarization favors an AFM coupling. This is quantitatively supported by Fig. 5(b). When the layer number of CrCl_3 increases, this difference gradually decreases, illustrating the ME effect is induced by the interfacial/proximity characteristics of ultra-thin vdW heterostructures.

Conversely, a macroscopic layer-dependent ME effect is observed in multilayer structures. As depicted in Fig. 5(a), for those heterostructures made by an odd layer number of CrCl_3 with an uncompensated AFM state, the overall magnetic moment per unit cell switches between $3 \mu_B$ and $9 \mu_B$ with the reversal of the FE polarization. This is the same as the heterobilayer result. However, for those heterostructures made by an even number of CrCl_3 layers with a compensated AFM state, switching the FE order does not alter the total magnetic moment. This is because the interlayer magnetic order between CrCl_3 layers remains AFM although the microscopic magnetic moment direction (Néel vector) of CrCl_3 layers is switched.

Acknowledge:

X.X. is supported by National Science Foundation (NSF) Designing Materials to Revolutionize and Engineer our Future (DMREF) DMR-2118779. L.Y. is supported by NSF DMR-2124934. The simulation used Anvil at Purdue University through allocation DMR100005 from the Advanced Cyberinfrastructure Coordination Ecosystem: Services & Support (ACCESS) program, which is supported by National Science Foundation grants #2138259, #2138286, #2138307, #2137603, and #2138296.

References:

- [1] T. Kimura, T. Goto, H. Shintani, K. Ishizaka, T. Arima, and Y. Tokura, Magnetic control of ferroelectric polarization. *Nature (London)* **426**, 55 (2003).
- [2] K. Cao, G. C. Guo, D. Vanderbilt, and L. He, First-Principles modeling of multiferroic RMn_2O_5 . *Phys. Rev. Lett.* **103**, 257201 (2009).
- [3] Y. Weng, L. Lin, E. Dagotto, and S. Dong, Inversion of ferrimagnetic magnetization by ferroelectric switching via a novel magnetoelectric coupling. *Phys. Rev. Lett.* **117**, 037601 (2016).
- [4] E. V. Boström, T. S. Parvini, J. W. McIver, A. Rubio, S. V. Kusminskiy, and M. A. Sentef, Direct optical probe of magnon topology in two-dimensional quantum magnets. *Phys. Rev. Lett.* **130**, 026701 (2023).
- [5] T. Hu and E. Kan, Progress and prospects in low-dimensional multiferroic materials. *WIREs Comput. Mol. Sci.* **9**, e1409 (2019).
- [6] S. Dong, H. Xiang, and E. Dagotto, Magnetoelectricity in multiferroics: a theoretical perspective. *Natl. Sci. Rev.* **6**, 629 (2019).
- [7] D. Khomskii, Classifying multiferroics: mechanisms and effects. *Physics*, **2**, 20 (2009).
- [8] C. Lu, M. Wu, L. Lin, and . Liu, Single-phase multiferroics: new materials, phenomena, and physics. *Natl. Sci. Rev.* **6**, 653 (2019).
- [9] N. A. Spaldin and R. Ramesh, Advances in magnetoelectric multiferroics. *Nat. Mater.* **18**, 203 (2019).
- [10] J. Wang, J. B. Neaton, H. Zheng, V. Nagarajan, S. B. Ogale, B. Liu, D. Viehland,

- V. Vaithyanathan, D. G. Schlom, U. V. Waghmare, N. A. Spaldin, K. M. Rabe, M. Wuttig, and R. Ramesh, Epitaxial BiFeO₃ multiferroic thin film heterostructures. *Science* **299**, 1719 (2003).
- [11] P. Jarillo-Herrero, S. Sapmaz, C. Dekker, L. P. Kouwenhoven, and H. S. Van Der Zant, Electron-hole symmetry in a semiconducting carbon nanotube quantum dot. *Nature (London)* **429**, 389 (2004).
- [12] J. Zhang, L. Lin, Y. Zhang, M. Wu, B. I. Yakobson, and S. Dong, Type-II multiferroic Hf₂VC₂F₂ MXene monolayer with high transition temperature. *J. Am. Chem. Soc.* **140**, 9768 (2018).
- [13] C. Xu, P. Chen, H. Tan, Y. Yang, H. Xiang, and L. Bellaiche, Electric-field switching of magnetic topological charge in type-I multiferroics. *Phys. Rev. Lett.* **125**, 037203 (2020).
- [14] J. Zhang, X. Shen, Y. Wang, C. Ji, Y. Zhou, J. Wang, F. Huang, and X. Lu, Design of two-dimensional multiferroics with direct polarization-magnetization coupling. *Phys. Rev. Lett.* **125**, 017601 (2020).
- [15] N. Hur, S. Park, P. A. Sharma, J. S. Ahn, S. Guha and S-W. Cheong, Electric polarization reversal and memory in a multiferroic material induced by magnetic fields. *Nature* **429**, 392 (2004).
- [16] R. Ramesh and N. A Spaldin, Multiferroics: progress and prospects in thin films. *Nat. Mater.* **6**, 21 (2007);
- [17] Q. Song, C. A. Occhialini, E. Ergeçen, B. Ilyas, D. Amoroso, P. Barone, J. Kapteghian, K. Watanabe, T. Taniguchi, A. S. Botana, S. Picozzi, N. Gedik, and R. Comin, Evidence for a single-layer van der Waals multiferroic. *Nature* **602**, 601 (2022).
- [18] Q. Yang, T. Zhong, Z. Tu, L. Zhu, M. Wu, and X. C. Zeng, Design of single-molecule multiferroics for efficient ultrahigh-density nonvolatile memories. *Adv. Sci.* **6**, 1801572 (2019).
- [19] H. Zheng, J. Wang, S. E. Lofland, Z. Ma, L. Mohaddes-Ardabili, T. Zhao, L. Salamanca-Riba, S. R. Shinde, S. B. Ogale, F. Bai, D. Viehland, Y. Jia, D. G. Schlom, M. Wuttig, A. Roytburd, and R. Ramesh, Multiferroic BaTiO₃-CoFe₂O₄ Nanostructures. *Science* **303**, 661 (2004).
- [20] L. Cao, X. Deng, G. Zhou, S. J. Liang, C. V. Nguyen, L. K. Ang, and Y. S. Ang,

Multiferroic van der Waals heterostructure $\text{FeCl}_2/\text{Sc}_2\text{CO}_2$: Nonvolatile electrically switchable electronic and spintronic properties. *Phys. Rev. B*, **105**, 165302 (2022).

[21] W. Sun, W. Wang, H. Li, G. Zhang, D. Chen, J. Wang, and Z. Cheng, Controlling bimerons as skyrmion analogues by ferroelectric polarization in 2D van der Waals multiferroic heterostructures. *Nat. Commun.* **11**, 5930 (2020).

[22] K. Huang, D. F. Shao, and E. Y. Tsymlal, Ferroelectric control of magnetic skyrmions in two-dimensional van der Waals heterostructures. *Nano Lett.* **22**, 3349 (2022).

[23] Y. Su, X. Li, M. Zhu, J. Zhang, L. You, and E. Y. Tsymlal, Van der Waals multiferroic tunnel junctions. *Nano Lett.* **21**, 175 (2021).

[24] C. Huang, J. Zhou, H. Sun, F. Wu, Y. Hou, and E. Kan, Toward room-temperature electrical control of magnetic order in multiferroic van der Waals materials. *Nano Lett.* **22**, 5191 (2022).

[25] X. Zhang, Z. Zhou, X. Yu, Y. Guo, Y. Chen, and J. Wang, Ferroelectric Control of Polarity of the Spin-polarized Current in Van Der Waals Multiferroic Heterostructures. *Adv. Funct. Mater.* **33**, 2301353 (2023).

[26] X. Xu, T. Zhang, Y. Dai, B. Huang, and Y. Ma, Electric-field switching of the antiferromagnetic topological state in a multiferroic heterobilayer. *Phys. Rev. B* **106**, 205307 (2022).

[27] W. Wang, W. Sun, H. Li, Y. Bai, F. Ren, C. You, and Z. Cheng, Nonvolatile magnetoelectric coupling in two-dimensional ferromagnetic-bilayer/ferroelectric van der Waals heterostructures, *Nanoscale* **13**, 14214 (2021).

[28] C. Huang, J. Zhou, H. Sun, F. Wu, Y. Hou, and E. Kan, Toward Room-Temperature Electrical Control of Magnetic Order in Multiferroic van der Waals Materials, *Nano Lett.* **22**, 5191 (2022).

[29] C. Gong, E. M. Kim, Y. Wang, G. Lee and X. Zhang, Multiferroicity in atomic van der Waals heterostructures. *Nat. Commun.* **10**, 2657 (2019).

[30] Y. Lu, R. Fei, X. Lu, L. Zhu, L. Wang, L. Yang, Artificial multiferroics and enhanced magnetoelectric effect in van der Waals heterostructures. *ACS Appl. Mater. Interfaces* **12**, 6243 (2020).

[31] B. Yang, B. Shao, J. Wang, Y. Li, C. Yam, S. Zhang, and B. Huang, Realization of

semiconducting layered multiferroic heterojunctions via asymmetrical magnetoelectric coupling. *Phys. Rev. B* **103**, L201405 (2021).

[32] H. Cheng, J. Zhou, C. Wang, W. Ji, and Y. Zhang, Nonvolatile electric field control of magnetism in bilayer CrI_3 on monolayer In_2Se_3 . *Phys. Rev. B* **104**, 064443 (2021).

[33] H. Tian, C. Xu, X. Li, Y. Yang, L. Bellaiche, and D. Wu, Band structure engineering of van der Waals heterostructures using ferroelectric clamped sandwich structures. *Phys. Rev. B* **103**, 125426 (2021).

[34] Y. Li, C. Liu, G. Zhao, T. Hu, and W. Ren, Two-dimensional multiferroics in a breathing kagome lattice. *Phys. Rev. B* **104**, L060405 (2021).

[35] G. Kresse and J. Furthmüller, Efficient iterative schemes for ab initio total-energy calculations using a plane-wave basis set. *Phys. Rev. B* **54**, 11169 (1996).

[36] J. P. Perdew, K. Burke, and M. Ernzerhof, Generalized gradient approximation made simple. *Phys. Rev. Lett.* **77**, 3865 (1996).

[37] G. Kresse and D. Joubert, From ultrasoft pseudopotentials to the projector augmented-wave method. *Phys. Rev. B* **59**, 1758 (1999).

[38] A. V. Krukau, O. A. Vydrov, A. F. Izmaylov, and G. E. Scuseria, Influence of the exchange screening parameter on the performance of screened hybrid functionals. *J. Chem. Phys.* **125**, 224106 (2006).

[39] P. Jiang, C. Wang, D. Chen, Z. Zhong, Z. Yuan, Z. Lu, and W. Ji, Stacking tunable interlayer magnetism in bilayer CrI_3 . *Phys. Rev. B* **99**, 144401 (2019).

[40] S. L. Dudarev, G. A. Botton, S. Y. Savrasov, C. J. Humphreys, and A. P. Sutton, Electron-energy-loss spectra and the structural stability of nickel oxide: An LSDA+U study. *Phys. Rev. B* **57**, 1505 (1998).

[41] See Supplemental Material at URL for the energy differences between interlayer AFM and FM coupling of $\text{CrCl}_3/\text{CCPS}$ under different U values and different stacking. We also provide the crystal structures of different stacking and NEB path.

[42] J. Neugebauer and M. Scheffler, Adsorbate-substrate and adsorbate-adsorbate interactions of Na and K adlayers on Al (111). *Phys. Rev. B* **46**, 16067 (1992).

[43] S. Grimme, S. Ehrlich, and L. Goerigk, Effect of the damping function in dispersion corrected density functional theory. *J. Comput. Chem.* **32**, 1456 (2011).

- [44] S. Guan, C. Liu, Y. Lu, Y. Yao, and S. A. Yang, Tunable ferroelectricity and anisotropic electric transport in monolayer β -GeSe. *Phys. Rev. B* **97**, 144104 (2018).
- [45] R. Resta and D. Vanderbilt, Theory of polarization: a modern approach. *Physics of Ferroelectrics* pp 31–68 (2007).
- [46] N. A. Spaldin, A beginner's guide to the modern theory of polarization. *J. Solid State Chem.* **195**, 2 (2012).
- [47] P. W. Anderson, Theory of superexchange interaction. *Phys. Rev.* **79**, 350 (1950).
- [48] J. B. Goodenough, Theory of the Role of Covalence in the Perovskite-Type Manganites [La, M(II)]MnO₃. *Phys. Rev.* **100**, 564 (1955).
- [49] J. Kanamori, Superexchange interaction and symmetry properties of electron orbitals. *J. Phys. Chem. Solids* **10**, 87 (1959).
- [50] Y. Lu, Y. Wang, L. Zhu, L. Yang, and L. Wang, Electric field tuning of magnetic states in single magnetic molecules. *Phys. Rev. B* **106**, 064405 (2022).
- [51] L. Webster and J. Yan, Strain-tunable magnetic anisotropy in monolayer CrCl₃, CrBr₃, and CrI₃. *Phys. Rev. B* **98**, 144411 (2018).
- [52] D. R. Klein, D. MacNeill, Q. Song, D. T. Larson, S. Fang, M. Xu, R. A. Ribeiro, P. C. Canfield, E. Kaxiras, R. Comin and P. Jarillo-Herrero, Enhancement of interlayer exchange in an ultrathin two-dimensional magnet. *Nat. Phys.* **15**, 1255 (2019).
- [53] Y. Lai, Z. Song, Y. Wan, M. Xue, C. Wang, Y. Ye, L. Dai, Z. Zhang, W. Yang, H. Dua and J. Yang, Two-dimensional ferromagnetism and driven ferroelectricity in van der Waals CuCrP₂S₆. *Nanoscale* **11**, 5163 (2019).
- [54] F. Xue, Y. Hou, Z. Wang, and R. Wu, Two-dimensional ferromagnetic van der Waals CrCl₃ monolayer with enhanced anisotropy and Curie temperature. *Phys. Rev. B* **100**, 224429 (2019).
- [55] K. Cho, S. Lee, R. Kalaivanan, R. Sankar, K. Choi, and S. Park, Tunable Ferroelectricity in Van der Waals Layered Antiferroelectric CuCrP₂S₆. *Adv. Funct. Mater.* **32**, 2204214 (2022).
- [56] Z. Wang, M. Gibertini, D. Dumcenco, T. Taniguchi, K. Watanabe, E. Giannini and A. F. Morpurgo, Determining the phase diagram of atomically thin layered antiferromagnet CrCl₃. *Nat. Nanotechnol.* **14**, 1116 (2019).

- [57] T. Song, Z. Fei, M. Yankowitz, Z. Lin, Q. Jiang, K. Hwangbo, Q. Zhang, B. Sun, T. Taniguchi, K. Watanabe, M. A. McGuire, D. Graf, T. Cao, J. Chu, D. H. Cobden, C. R. Dean, D. Xiao, and X. Xu, Switching 2D magnetic states via pressure tuning of layer stacking. *Nat. Mater.* **18**, 1298 (2019).
- [58] T. Li, S. Jiang, N. Sivadas, Z. Wang, Y. Xu, D. Weber, J. E. Goldberger, K. Watanabe, T. Taniguchi, C. J. Fennie, K. F. Mak, and J. Shan, Pressure-controlled interlayer magnetism in atomically thin CrI₃. *Nat. Mater.* **18**, 1303 (2019)
- [59] Z. Guan, H. Hu, X. Shen, P. Xiang, N. Zhong, J. Chu, and C. Duan, Recent progress in two-dimensional ferroelectric materials. *Adv. Electron. Mater.* **6**, 1900818 (2020).
- [60] J. Qi, H. Wang, X. Chen, and X. Qian, Two-dimensional multiferroic semiconductors with coexisting ferroelectricity and ferromagnetism. *Appl. Phys. Lett.* **113**, 043102 (2018).
- [61] F. Yao, V. Multian, Z. Wang, N. Ubrig, J. Teyssier, F. Wu, E. Giannini, M. Gibertini, I. Gutiérrez-Lezama and A. F. Morpurgo, Multiple antiferromagnetic phases and magnetic anisotropy in exfoliated CrBr₃ multilayers. *Nat Commun. Nat Commun.* **14**, 4969 (2023).
- [62] J. Hu, C. Duan, C. Nan, and L. Chen, Understanding and designing magnetoelectric heterostructures guided by computation: progresses, remaining questions, and perspectives. *NPJ Comput. Mater.* **3**, 18 (2017).
- [63] N. V. Srihari, K. B. Vinayakumar, and K. K. Nagaraja, Magnetoelectric coupling in bismuth ferrite—challenges and perspectives. *Coatings* **10**, 1221 (2020).
- [64] S. Dong, J.-M. Liu, S.-W. Cheong, and Z. Ren, Multiferroic materials and magnetoelectric physics: symmetry, entanglement, excitation, and topology. *Adv. Phys.* **64**, 519 (2015).
- [65] H. H. Kim, et al. Evolution of interlayer and intralayer magnetism in three atomically thin chromium trihalides. *Proc. Natl. Acad. Sci. USA* **116**, 11131 (2019).
- [66] C. Gong, et al. Discovery of intrinsic ferromagnetism in two-dimensional van der Waals crystals. *Nature* **546**, 265 (2017).
- [67] N. Liu, S. Schreyeck, K. M. Fijalkowski, M. Kamp, K. Brunner, C. Gould, and L. W. Molenkamp, Antiferromagnetic order in MnBi₂Te₄ films grown on Si (1 1 1) by molecular beam epitaxy. *J. Cryst. Growth* **591**, 126677 (2022).

- [68] H. Hrenberg, M. Wiesmann, J. Garcia-Jaca, H. Weitzel, and H. Fuess, Magnetic structures of the high-pressure modifications of CoMoO_4 and CuMoO_4 . *J. Magn. Magn. Mater.* **182**, 152 (1998).
- [69] N. Sivadas, S. Okamoto, X. Xu, Craig J. Fennie, and D. Xiao, Stacking-Dependent Magnetism in Bilayer CrI_3 . *Nano Lett.* **18**, 7658 (2018).
- [70] J. B. Goodenough, An interpretation of the magnetic properties of the perovskite-type mixed crystals $\text{La}_{1-x}\text{Sr}_x\text{CoO}_{3-\lambda}$. *J. Phys. Chem. Solids* **6**, 287 (1958).
- [71] M. Amini, A. O. Fumega, H. González-Herrero, V. Vaňo, S. Kezilebieke, J. L. Lado, and P. Liljeroth, Atomic-Scale Visualization of Multiferroicity in Monolayer NiI_2 . *Adv. Mater.* **36**, (2024).
- [72] F.Y. Gao, X. Peng, X. Cheng, et al. Giant chiral magnetoelectric oscillations in a van der Waals multiferroic. *Nature* **632**, 273 (2024).

Figures:

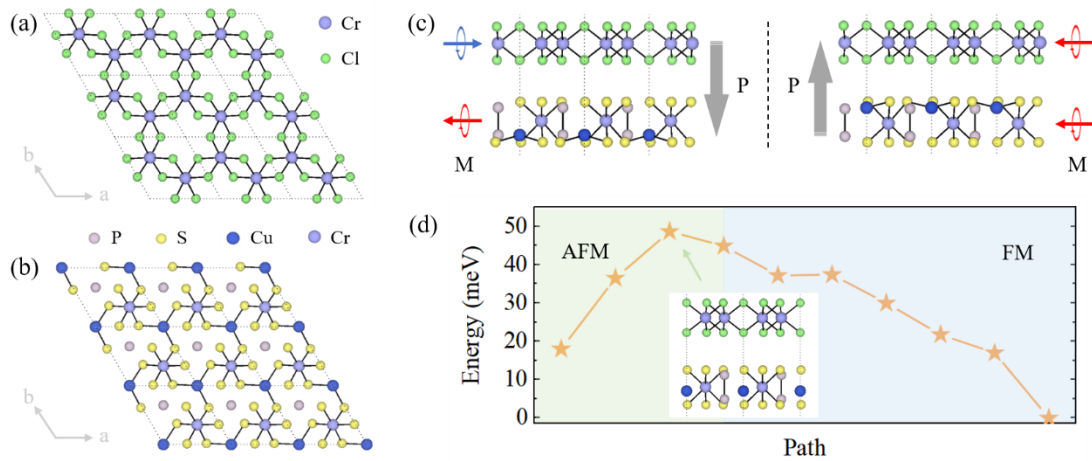


Fig. 1. (a) and (b) Top views of crystal structure of monolayer CrCl₃ and CCPS, respectively. (c) Side views of CrCl₃/CCPS heterobilayer under different electric polarization. Large arrows represent the electric polarization direction, while small arrows represent the magnetic configuration. (d) FE transition pathway between polarization-down (AFM) and polarization-up (FM). The background color illustrates the ground-state interlayer magnetic order in those transition structures.

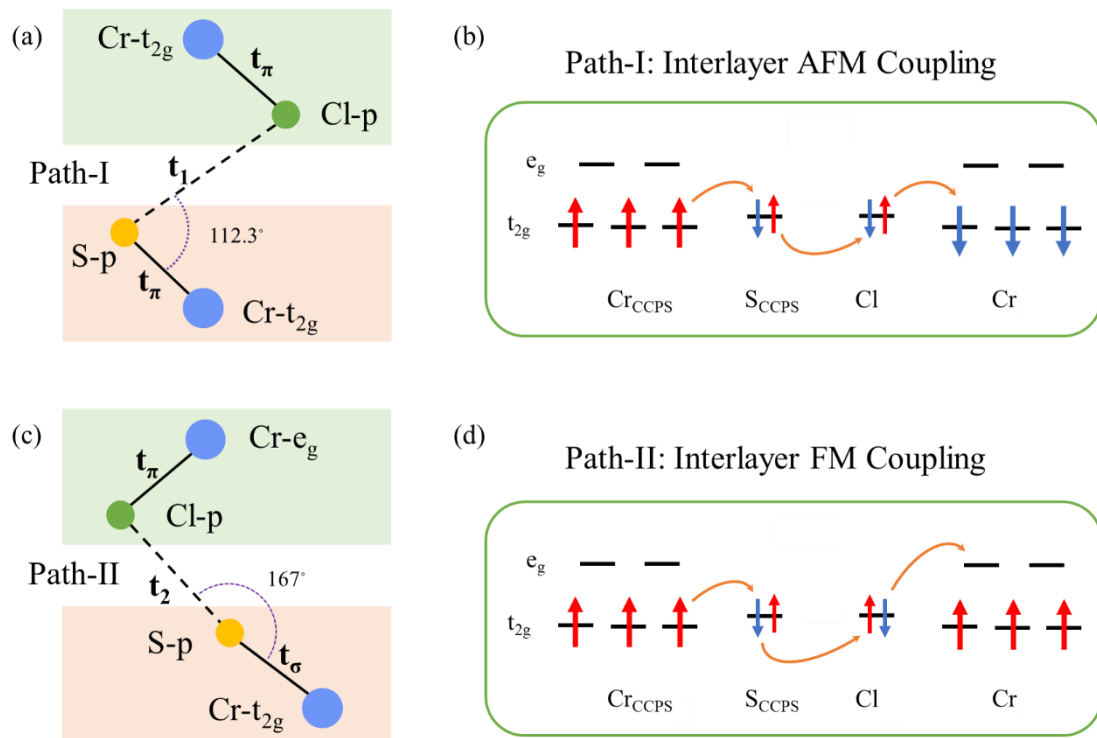


Fig. 2. (a) Schematic of interlayer super-super-exchange AFM path I. (b) Corresponding interlayer hoppings between spin states of path I. (c) Schematic of interlayer super-super-exchange FM path II. (d) Corresponding interlayer hoppings between spin states of path II.

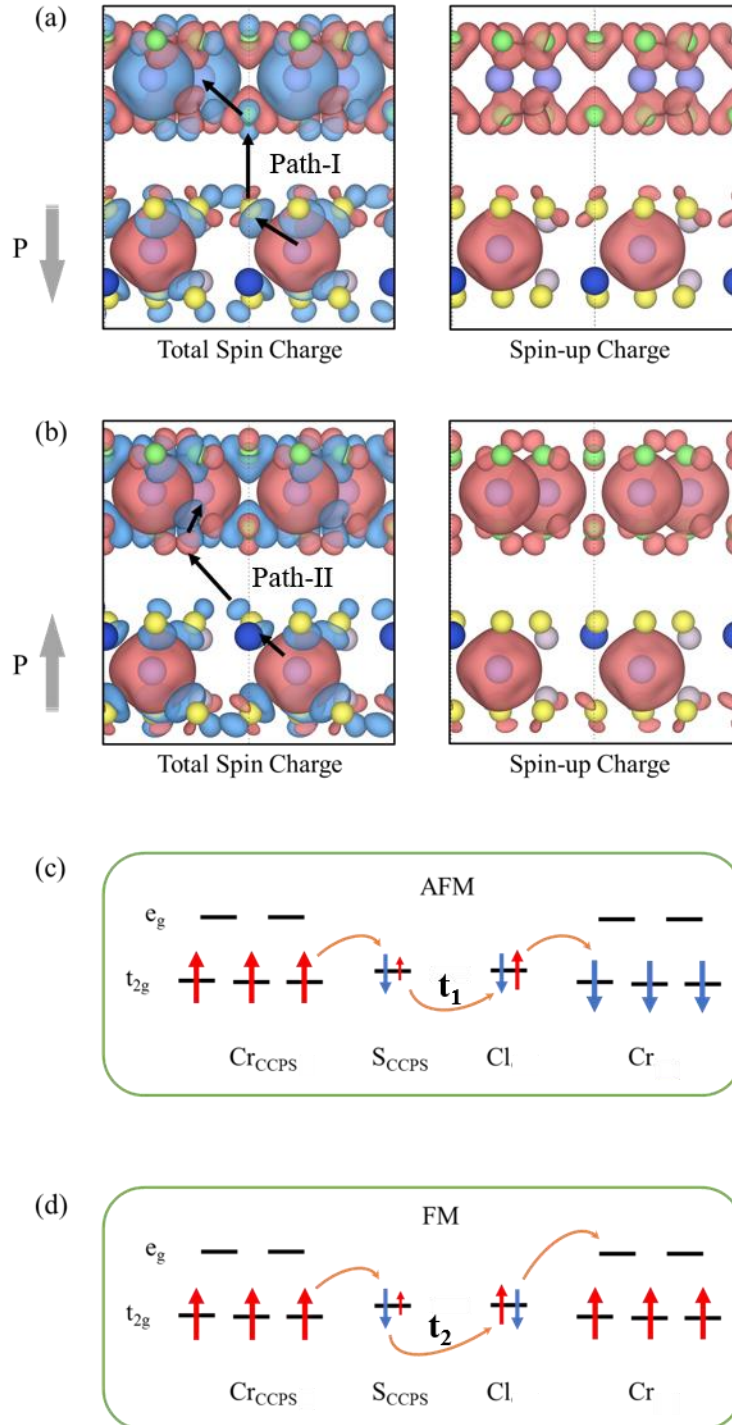


Fig. 3. (a) Left panel is the isosurface plot of total spin density of AFM-ground-state CrCl₃/CCPS under downward polarization. Right panel is the spin-up component. (b) Left panel is that of FM-ground-state CrCl₃/CCPS under upward polarization. Right panel is the spin-up component. The interlayer super-super-exchange paths are marked in left panels. The red and blue colors represent spin-up and spin-down components, respectively. The isosurface value is set to be 0.5% of the maximum value. (c) and (d) Schematics of AFM (path-I) and FM (path-II) interlayer hopping paths, respectively.

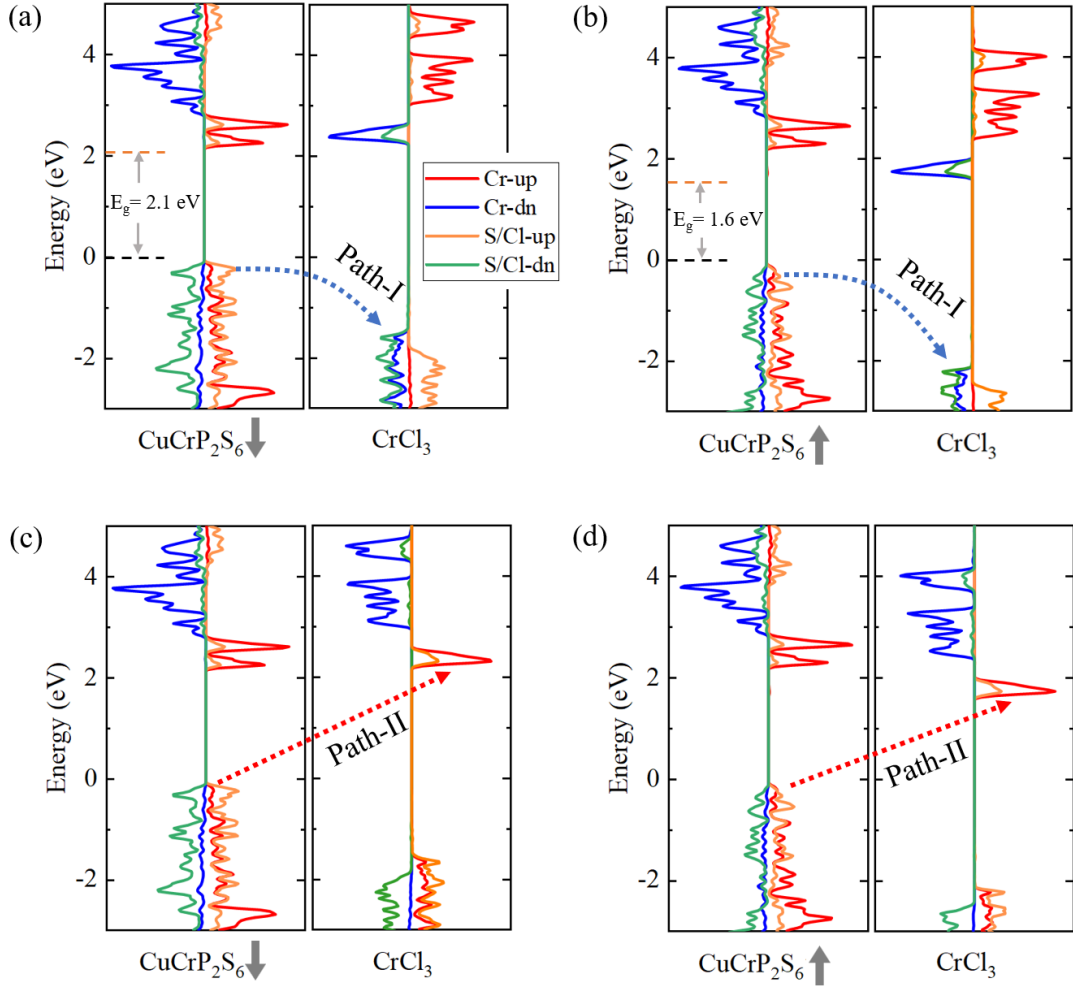


Fig. 4. (a) and (b) PDOS without SOC of AFM CrCl₃/CCPS heterostructures under downward and upward polarizations, respectively. (c) and (d) Those of AFM heterostructures under downward and upward polarization, respectively. The energy of the valence band maximum is set to be zero. The band gap and hopping paths are marked to direct readers' eyes.

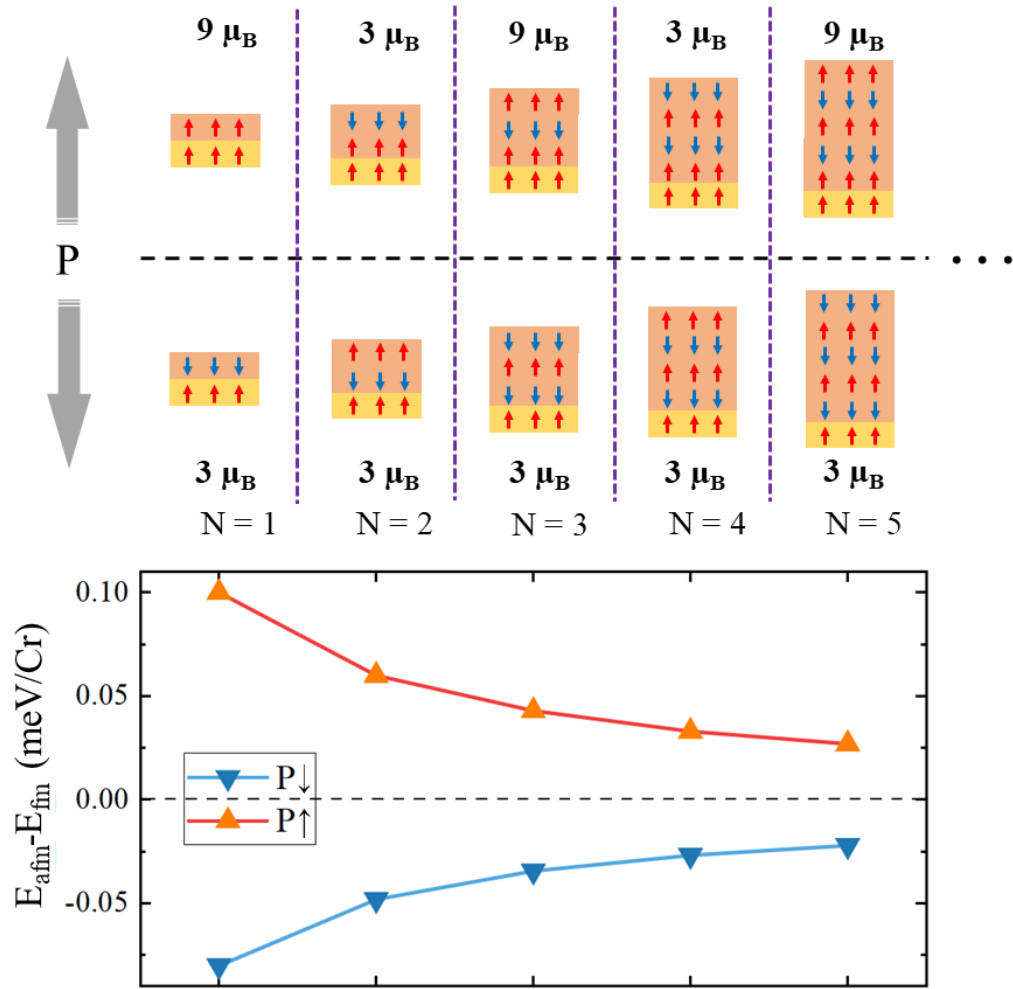


Fig. 5. (a) Ground-state interlayer magnetic configurations according to the CrCl₃ layer number (N) under opposite polarizations of CCPS. The bottom layer is fixed to be CCPS. The net magnetic moment per unit cell is listed for each configuration. (b) Corresponding total-energy differences between AFM and FM couplings according to the CrCl₃ layer number under opposite polarizations.